# Chapter 4

# Exploring $C_{24}$ Fullerene as an illicit Drug sensor

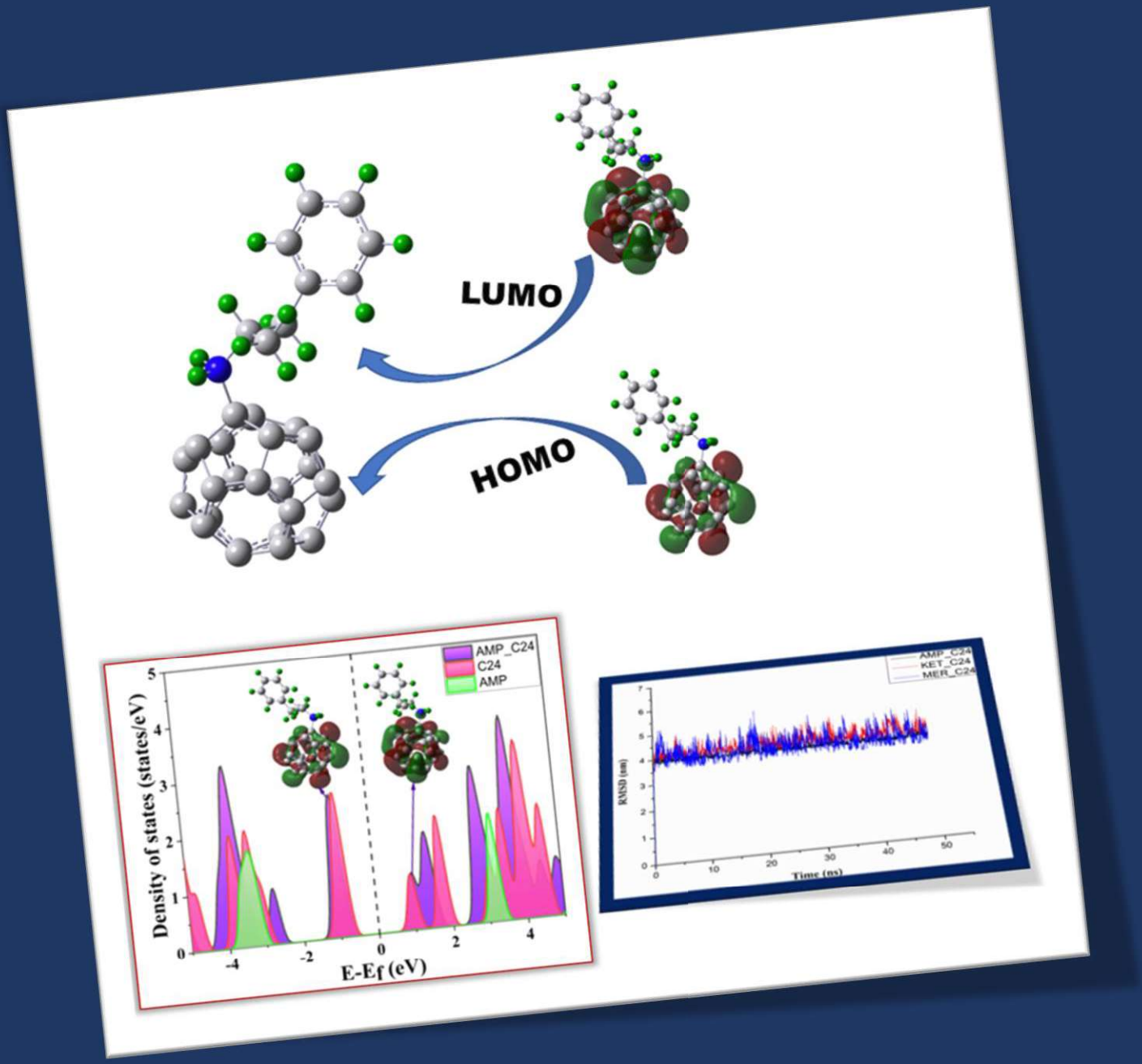

## 4.1 Introduction

Concern over tainted pharmaceutical goods is on the rise, and there is now a global issue and conundrum around the pharmaceutical industry's dubious clinical obligations. An accurate evaluation of a medicine's active component content determines the quality of the drug[1]. Identifying and handling illicit drugs, particularly synthetic ones, is a significant and pressing issue in today's world. This challenge poses a threat to social unity, family stability, and human well-being[2-3]. The overdose of some of the drugs can lead to fatal human life, the renowned abuse drugs such as Amphetamine (**AMP**), Ketamine (**KET**) and Mercaptopurine (**MER**). It is very important for drug communities and security agencies alike to detect the drug molecule AMP in biological samples as it is a popular drug that is misused and is used in many ways. Excessive consumption of it leads to various critical issues, including psychological disturbances and an increased risk of traffic accidents. [4]. There is a second fatal drug molecule, KET, which enkindles NMDA receptors on neuronal cells, hence causing hallucinations[5]. Due to the hallucinogenic effects of its excessive use, a K-hole occurs in the human body, resulting in a cataleptic state[6-7]. MER, the last drug from the above group, exhibits immunosuppressive properties and is used for treating acute lymphoblastic leukaemia[8]. Pregnant women are prohibited from taking MER, as described in the previous report. This drug causes abnormal abortion rates during the first trimester of pregnancy[9]. Its cytotoxic nature also limits its application due to several side effects[10]. It's hard to detect these spike drugs because they are queered into quenchers to incapacitate victims, as well as because of their low concentrations and complex sample matrices. For the medical field and for the prevention and reduction of drug-related crimes, it is of great importance to increase research, impressionable, rapid, and inexpensive methods for the detection of illicit drugs[11]. The detection of the drugs has been accomplished using a wide variety of techniques, including high-performance liquid chromatography (HPLC)[12], GCM[13], capillary electrophoresis[14], ion mobility spectrometry[15], UV-visible spectrophotometry[16], electrochemical luminescence[17], Raman spectrometry[18], fluorescence[19], and film-based fluorescent[20]. Despite their time-consuming and expensive instrumentation, most of the techniques mentioned above have been confirmed to rigorous use[11]. Since electrochemical sensors offer a number of advantages, including cost-effectiveness, portability, simplicity, speed, and sensitivity[21], they are an excellent alternative to conventional sensors. A state-of-the-art density functional theory (DFT) approach has been used to detect unscriptural drugs

using nanomaterials of low dimension. AMP drug adsorption behavior over pristine and doped $Al_{12}N_{12}$ and $Al_{12}P_{12}$ nanocages[22], intrinsic and extrinsic $C_{60}$ fullerenes[23], Al-doped ZnO nanotubes[24], silicon carbide nanotubes[25], AlN nano-cage[26], and $BC_3$ nanotubes and nanosheets[27] has been studied by theoretical studies. A number of different materials have been used to investigate the sensing mechanism of MER drug, such as pristine and doped $C_{70}$ fullerenes[28], boron nitride nanocages[29], BN nanotubes, nanosheets, and clusters[30], as well as $B_{12}N_{12}$, $AlB_{11}N_{12}$ and $GaB_{11}N_{12}$ nanoclusters[31]. R. Zhiani and colleagues undertook a joint study employing both Density Functional Theory (DFT) and Molecular Dynamics (MD) simulations to investigate KET drug detection using functionalized single-walled carbon nanotubes[32]. As compared to other carbon-based nanomaterials like graphene and CNTs, fullerenes have recently received a great deal of attention due to their low side effects in biological media, their high surface area and hydrophobic nature[33-34]. The $C_{24}$ in Comparison to $C_{60}$, $C_{20}$, and doped $C_{20}$ demonstrates the better sensitivity due to its lower energy band gap[23][35]. As we can see from our literature review, the stability of $C_{24}$ fullerene has proved to be an important factor to ensure its success as a drug carrier and sensor. To the best of our knowledge no systematic study has been conducted on the adsorption of Amphetamine (AMP), Ketamine (KET) and Mercaptopurine (MER) over carbon nanostructures using MD simulations. Using classical MD simulations and DFT theories, we have investigated sensing applications of the pristine $C_{24}$ fullerene for the above-mentioned drug molecules. In order to determine whether the pristine $C_{24}$ fullerene is suitable for sensing, we conducted DFT as well as classical MD simulations on the above-mentioned drug molecules. Additionally, a DFT investigation was conducted to assess the binding mechanisms and sensitivity of three drug molecules when interacting with $C_{24}$ fullerene, both in a gaseous environment and under the influence of solvent effects. A DFT study was also used to analyse electronic features such as NBO, Mulliken charge, and DOS. Classical molecular dynamics (MD) simulations were employed to explore the stability and the formation or breaking of bonds within complexes of drug molecules and fullerene at a temperature of 310K (room temperature).

## 4.2 Computational Details:

### 4.2.1 Details of the DFT calculation

The structural refinement of both the drug molecules and $C_{24}$ fullerene, along with electronic computations, were conducted using the Gaussian 09 software package[36] were performed using the DFT/B3LYP technique employing the 6-31G(d,p) basis set together with the D3 version of Grimme's dispersion[37]. The adsorption energy, $E_{ad}$ is defined as

$$E_{ad} = E_{C24/Drug\ Molecules} - (E_{C24} + E_{Drug\ Molecules}) \ldots\ldots\ldots\ldots (1)$$

Here, $E_{Drug\ Molecules}$ and $E_{C24/Drug\text{-}\ Molecules}$ are the energies of the isolated drug molecules and optimized $C_{24}$ fullerene with the adsorbed drug molecules, respectively. $E_{C24}$ corresponds to the energy of the optimized $C_{24}$ fullerene. The difference between the lowest unoccupied molecular orbital (LUMO) and highest molecular orbital (HOMO), which is known as the HOMO-LUMO energy gap $E_G$, is written as

$$E_G = E_{LUMO} - E_{HOMO} \ldots\ldots\ldots\ldots\ldots\ldots\ldots (2)$$

### 4.2.2 Details of the MD Simulation

We employed a classical molecular dynamics simulation, utilizing the GROMACS package version 5.0.2[38] and the CHARRM27 force field [39], to validate the adsorption behaviour of drug molecules Amphetamine (AMP), Ketamine (KET), and Mercaptopurine (MER) on the external surface of $C_{24}$ fullerene. Three simulation systems are developed ($C_{24}$/AMP, $C_{24}$/KET, and $C_{24}$/MER). **Table 4.6** lists details of all investigated systems. It is shown that the TIP3P model can be used to describe the structure of water molecules[40]. For the MD simulation, we employed the ultimate optimized structures derived from our DFT computations. These structures were then converted into PDB format via GaussView 5. To account for periodic boundary conditions, we ensured that all simulation boxes were sufficiently large, thereby mitigating interactions between components and neighbouring cells. It's important to highlight that in each of the containers, the drug molecules were positioned approximately 1.5-2 Å apart from the surfaces of the $C_{24}$ fullerenes. Prior to equilibrating the systems using NVT and NPT ensembles for 100 picoseconds, a preliminary minimization stage was performed on the entire system.By using V-rescale and Berendsen algorithms, the pressure and temperature are kept constant at 310 K and 1 bar respectively[41]. Production MD runs with a step time of 2fs have been carried out for each system for 50ns under periodic conditions. The LINCS method has

been employed[42] to constrain all bonds to their equilibrium length. Long-range electrostatic interactions have been treated using the particle-mesh Ewald (PME) approach, and non-bonded interactions are estimated with a 1.2 nm range cut-off [43]. The molecular visualization is done using the Visual Molecular Dynamics (VMD) program[44].

## 4.3 Results and Discussion

### 4.3.1 DFT calculation results

#### 4.3.1.1 Geometry Optimization of the adsorbent $C_{24}$ fullerene and Drug molecules

This section seeks to provide a thorough explanation of how the three chosen drug molecules interact with $C_{24}$ fullerene. Using DFT-D3/B3LYP,6-31G(d,p), all of the chosen molecular structures, including $C_{24}$ fullerene and all three drug molecules, were relaxed in the first step. The optimized geometries are depicted in **Figure 4.1**. The $C_{24}$ fullerene with a $D_{6h}$ point group has one hexagonal ring at the top and one at the bottom, and twelve pentagonal rings in the centre. The optimal bond lengths for C=C and C-C are 1.36 Å and 1.52 Å, while Energy gap ($E_G$) is 1.82 eV with HOMO and LUMO energies of -5.65 and -3.83 eV, respectively (see **Table 4.1**). The optimized bond lengths and energy gap are largely in line with the available data[45]. The calculation of the formation energy, which was determined to be -8.29 eV/atom, revealed the structural stability of $C_{24}$, which is consistent with existing literature[46-47]. The formation energy is highly negative, which ensures stability. In addition, vibrational modes have been calculated to confirm stability with infrared frequencies, and there is no imaginary frequency present. Vibrational frequencies vary between 200 and 1600 $cm^{-1}$, which is consistent with Hossian et.al. [46]. We optimized the drug molecules after confirming the basic properties of $C_{24}$. It is necessary to have a precise representation of the charge population of the drug molecules in order to better understand their binding affinity and interaction with $C_{24}$. As such, **Figure 4.2** illustrates the calculated Molecular Electrostatic Potential (MESP) for the aforementioned drug molecules and fullerene $C_{24}$. A colour scheme has been chosen in such a way that the red part represents attractive potential and the blue part represents repulsive potential. $C_{24}$ fullerenes contain intermediate negative portions over both hollow pentagonal and hexagonal rings, making them ideal candidates for nucleophilic attack sites. Due to the lone pair electrons of nitrogen atoms, a high negative electron density surface is visible along the nitrogen atom's $NH_2$ group and an intermediate negative region along the other group of AMP drug. In addition, KET and MER molecules contain regions with high

electron density along oxygen and sulphur atoms. The structures of $C_{24}$, AMP, KET, and MER molecules do not change significantly when optimized in water.

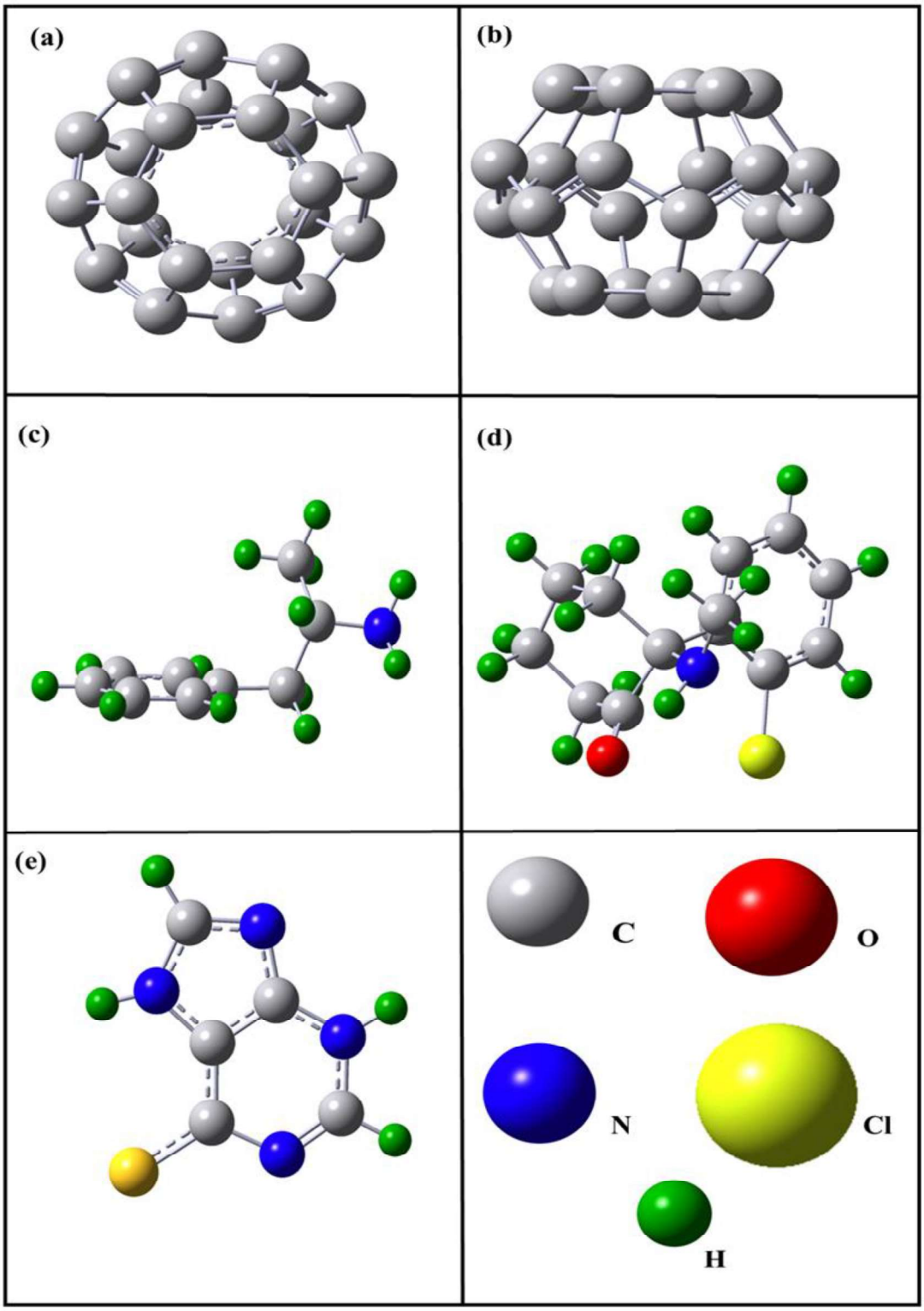


**Figure 4.1:** *Optimized geometry of $C_{24}$ fullerene (top(a) and side view (b)) and drug molecules (AMP (c), KET (d),) and MER (e)).*

### 4.3.1.2 Interaction characteristics of Amphetamine (AMP), Ketamine (KET) and Mercaptopurine (MER) drug molecules onto $C_{24}$ fullerene

In this study, we analysed the most stable configuration of drug molecules interacting with $C_{24}$ fullerene to verify their affinity towards $C_{24}$ fullerene (**Figure 4.3**). A study shows that the drug molecules are adsorbable over hexagonal or pentagonal rings of the $C_{24}$ fullerene without any structural distortion. A number of possible adsorption sites were explored for the drug. Several possible adsorption sites have been proposed for the drug molecules on $C_{24}$ in order to find the minimum energetic conformer. As a result of the additional electrons present,

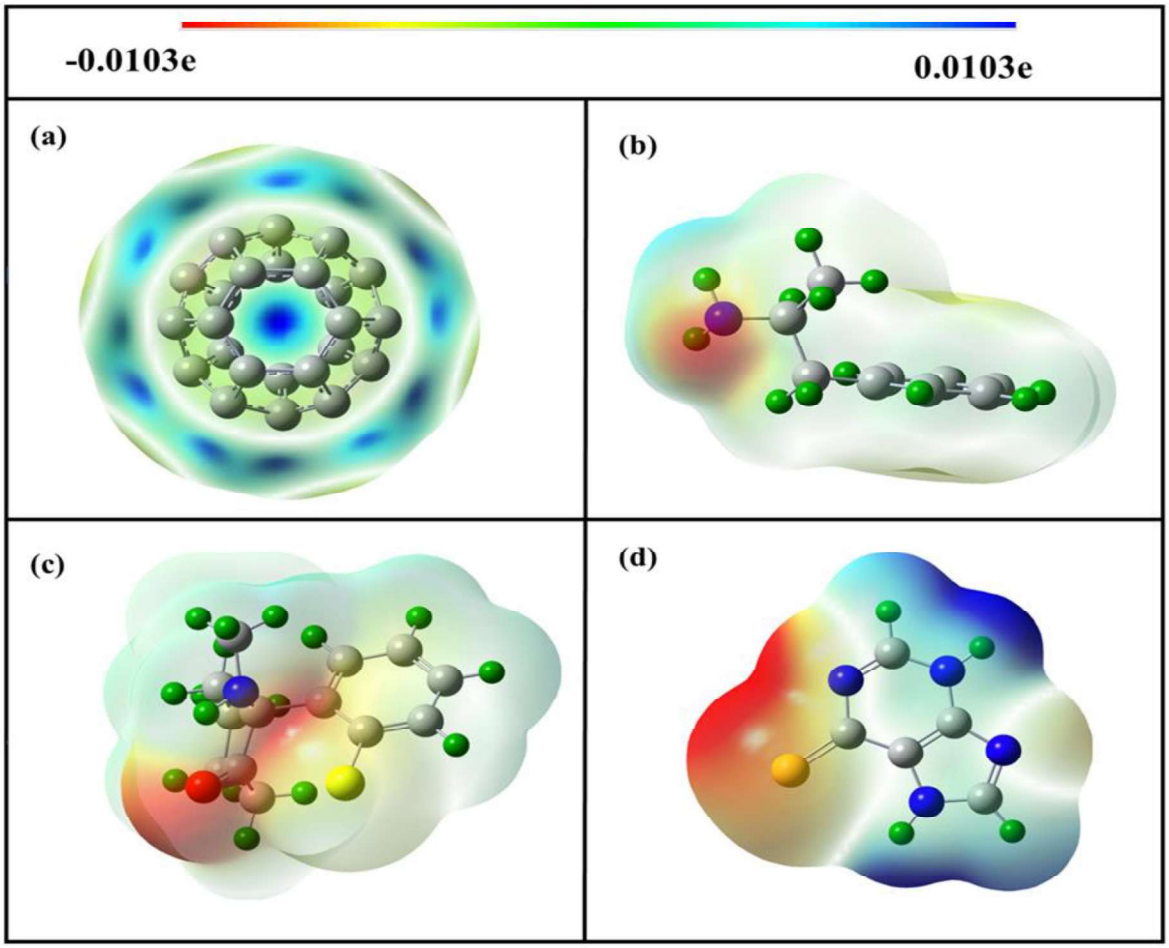


**Figure 4.2***: Electrostatic potential (ESP) maps for $C_{24}$ fullerene (a) and drug molecules AMP (b), KET (c), and MER (d) (EPS values ranging from -0.0103e to 0.0103e).*

N-atoms are preferred over H-atoms for drug adsorption onto $C_{24}$, and consistent with the results of MESP analysis. The distance between the nitrogen (N) atom of AMP and the carbon (C) atom of $C_{24}$ is roughly 1.55 Å, and the drug molecule AMP's adsorption energy onto $C_{24}$ is

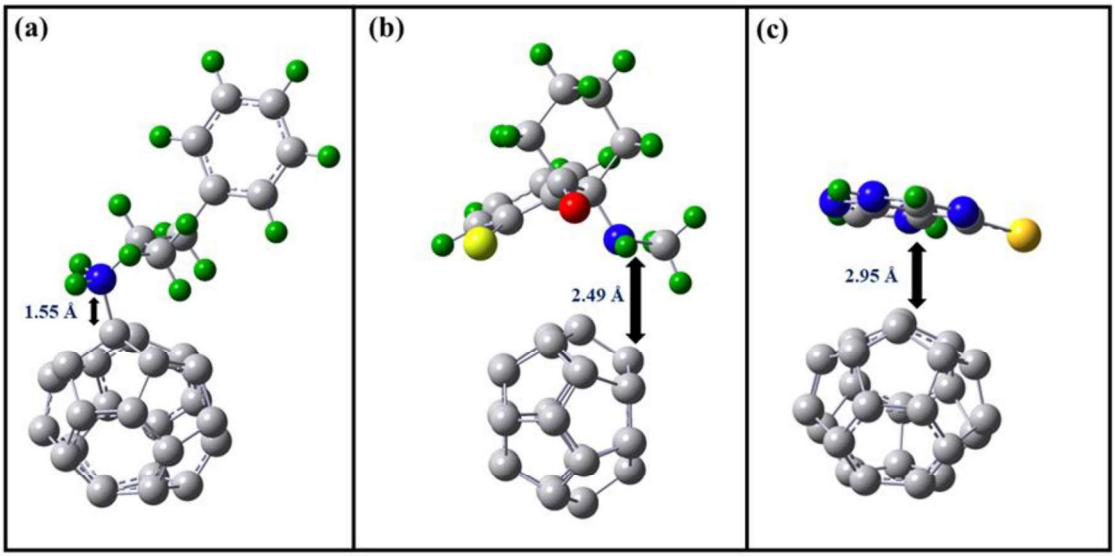


**Figure 4.3** *: The lowest-energy configurations of AMP (a), KET (b), and MER (c) when adsorbed onto $C_{24}$ fullerene, respectively.*

-1.02 eV (see **Table 4.1**). Chemisorption is the process by which the AMP molecule is strongly adsorbed on the $C_{24}$ fullerene[48]. With -0.423 eV energy, KET drug molecule adsorbed over the pentagonal ring of $C_{24}$ and optimized separation between **KET** drug molecule and $C_{24}$ fullerene is 2.49 Å, which indicates its physisorption mechanism. Adsorption of the MER drug molecule occurs through physisorption over the hexagonal site of fullerene $C_{24}$[35]. The MER drug molecule and $C_{24}$ fullerene are separated by a minimum of 2.95 Å atom to atom. The adsorption energies reveal its nature and the sequence or tendency of drug molecules towards the fullerene.

**Table 4.1:** *Calculated value of Adsorption energy ($E_{ad}$), LUMO energy ($E_{LUMO}$), Fermi level ($E_F$), HOMO energy ($E_{HOMO}$), HOMO-LUMO gap ($E_G$), relative change in $E_F$ ($\Delta E_{FR}$), relative change in $E_G$ ($\Delta E_{GR}$) and adsorption distance(d) of AMP, KET and MER adsorbed over $C_{24}$ fullerene, respectively.*

| System | $E_{ad}$ (eV) | $E_{LUMO}$ (eV) | $E_F$ (eV) | $E_{HOMO}$ (eV) | $E_G$ (eV) | $\Delta E_{FR}$ (%) | $\Delta E_{GR}$ (%) | d (Å) |
|---|---|---|---|---|---|---|---|---|
| $C_{24}$ | … | -3.83 | -4.74 | -5.65 | 1.82 | …… | ….. | ……. |
| AMP/$C_{24}$ | -1.02 | -2.47 | -3.42 | -4.37 | 1.90 | -27.85 | 4.39 | 1.55 |
| KET/$C_{24}$ | -0.423 | -3.23 | -4.13 | -5.02 | 1.79 | -12.87 | -1.65 | 2.49 |
| MER/$C_{24}$ | -0.365 | -3.69 | -4.58 | -5.46 | 1.77 | -3.37 | -2.74 | 2.95 |

#### 4.3.1.3 The natural bond orbital (NBO) charge analysis

The ability to better comprehend how adsorbate and adsorbent interact is made possible by the electronic charge transfer, which is a crucial component. The NBO analysis, which is displayed in **Table 4.2**, can be used to explain the charge transfer between drug molecules and $C_{24}$ in their ideal geometrics throughout the adsorption process[49]. We also examined the NBO($Q_N$)[50] and Mulliken charge transfer ($Q_M$)[50-51] between the drug molecules and $C_{24}$ fullerene to ascertain the path of charge transfer within the molecule-molecule interactions. Our results from the Mulliken charge analysis ($Q_M$) are consistent with the positive value of $Q_N$ that we obtain. These were also noted in earlier literature[51] , and it is believed that charge was transferred from drug molecules to $C_{24}$ fullerene. The charge distribution of drug molecules adsorbed over $C_{24}$ is shown in **Figure 4.4**. Additionally, the NBO calculation has been used to clarify the second-order perturbation stabilization energy, $E^{(2)}$, of the donor-acceptor (bond-antibond) interaction between the $C_{24}$ fullerene and drug molecules, which was predicted by the second-order Fock matrix[49]. For the delocalization of the donor (i) to the acceptor (j), the equation of second order perturbation stabilization energy, $E^{(2)}$, is represented as

$$E^{(2)} = \Delta E_y = q_i \frac{F^{(2)}(ij)}{\varepsilon_i - \varepsilon_j} \ldots\ldots\ldots\ldots\ldots\ldots\ldots\ldots (3)$$

The second order perturbation stabilization energy is directly correlated with the NBO interacting intensity, and it is well known that a stronger interaction between the donor and acceptor results in a higher stabilization energy, which confers more stability for $C_{24}$/drug-molecule complexes. The greatest $E^{(2)}$ values are shown in **Table 4.2**. According to the obtained

**Table 4.2:** *The NBO second-order perturbation energy ($E^2$, kcal/mol) corresponds to the charge transfer between the $C_{24}$ fullerene and AMP, KET, and MER, respectively.*

| System | Donor | Acceptor | $E^2$ (Kcal/mol) |
|---|---|---|---|
| **AMP/$C_{24}$** | BD(C3-C6) | BD*(N25-C26) | 46.40 |
| **KET/$C_{24}$** | LP(N27) | BD*(C7-C15) | 9.33 |
| **MER/$C_{24}$** | BD*(C30-C31) | BD*(C9-C10) | 2.60 |

results, the intermolecular interaction in the AMP/$C_{24}$ complex identifies the interaction as (C3-C6) of $C_{24}$ fullerene functions as donor while (N25-C26) of AMP acts as acceptor, which is compatible with the results of ESP. The highest value of $E^{(2)}$ is 46.40 kcal/mol, indicating that there is strongest interaction between the AMP drug and the $C_{24}$ fullerene. Chemisorption is taking place which confirms from the charge transfer and adsorption energy of AMP over $C_{24}$ fullerene. The greatest values of $E^{(2)}$ for the complexes $C_{24}$/KET and $C_{24}$/MER are 9.33 and 2.60 Kcal/mol, respectively. The lower values in comparison to the AMP/$C_{24}$ combination support the physisorption nature of their adsorption. In general, it may be said that most interactions take place between the donor orbitals of the drug molecule and the acceptor orbitals of pristine $C_{24}$.

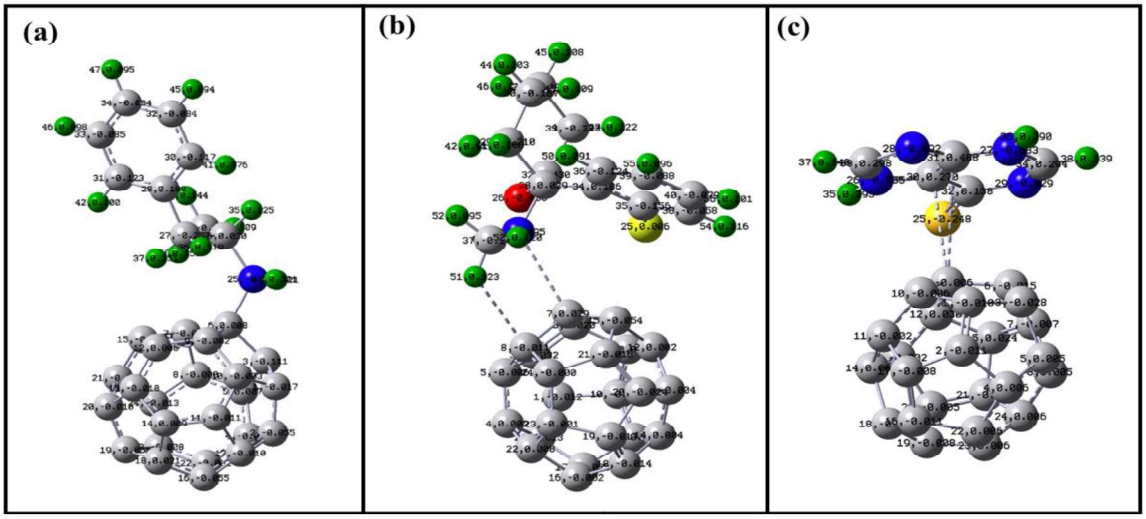


**Figure 4.4:** *Mulliken charge distribution analysis for AMP (a), KET (b), and MER (e) when adsorbed onto $C_{24}$ fullerene, respectively.*

#### 4.3.1.4 Density of states (DOS)

The change in the HOMO and LUMO levels, which causes the charge transfer process, provides evidence of the drug-system interaction. As a result, we generated the density of states using GaussSum software and calculated the energy gap of the systems using equation 2. To facilitate a comparison between the HOMO and LUMO levels of the pristine $C_{24}$ and their corresponding states when interacting with unaltered drugs, we computed the Fermi level. This was achieved by calculating half the sum of the HOMO and LUMO levels within the systems and setting it as the zero-reference point on the density of states plot. This enabled us to assess the changes in the HOMO and LUMO levels of pristine $C_{24}$ following their interaction. Two

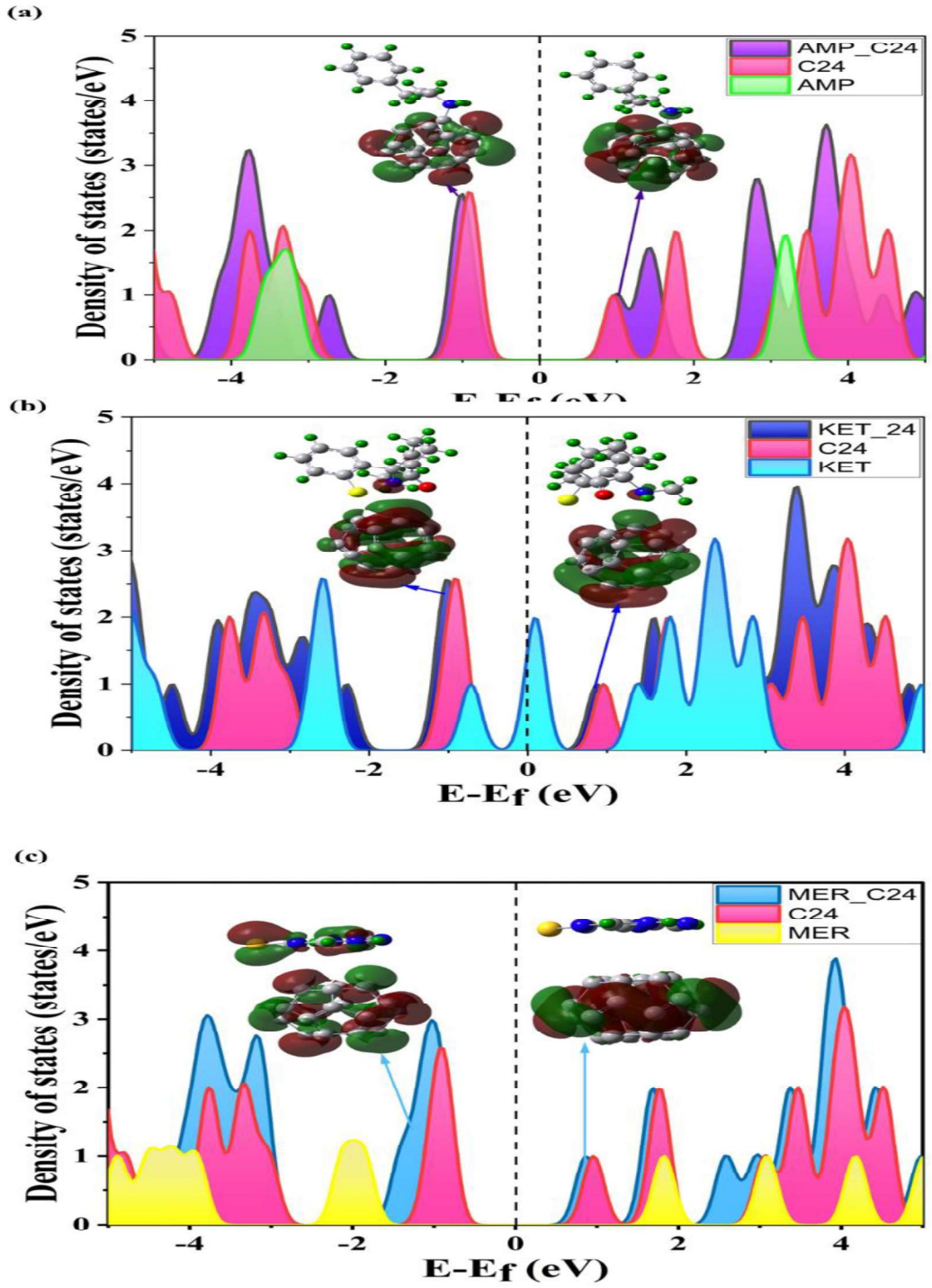


**Figure 4.5:** *Density of states for the interaction between $C_{24}$ fullerene and AMP (a), KET (b), and MER (c).*

other parameters that affect the energy gap are the system stability and chemical reactivity. Higher energy gap corresponds to high kinetic stability, which in turn denotes low chemical reactivity, and vice versa. The confirmed energy gap of $C_{24}$ is 1.82 eV, which is consistent with

our earlier research[35] and with previously reported works[45]. The energy gaps for the drug molecules AMP, KET, and MER are 6.24 eV, 5.18 eV, and 3.69 eV, respectively. Higher energy gaps suggest that electrons from the low-lying HOMO must be transferred to the high-lying LUMO, which is energetically unfavourable and indicates that $C_{24}$ is highly reactive to these drugs. It's noteworthy to note that after analysing the density of states of $C_{24}$ interacting with these three drugs, we found that the energy gap of the complex that was created after $C_{24}$ interacted with AMP showed an increase. Based on the shift of the HOMO and LUMO levels to negative values, the energy bands of these systems increase compared to the $C_{24}$ molecules (**Figure 4.5**). We notice the greatest change in HOMO level in the AMP instance, as well as the localization of both HOMO and LUMO at $C_{24}$ fullerene. This change in HOMO and LUMO and the Mulliken charge analysis conclude that there is charge transfer from $C_{24}$ fullerene to the AMP drug molecule. In comparison to the KET and MER complex configurations, the $E_G$ corresponds to the AMP complex configuration having the highest value. However, we find that the MER complex configuration has the smallest energy gap compared to the other two complex configurations due to the lowest negative values for HOMO and LUMO (see Table-1). In the case of the MER and KET complexes, we also notice that the HOMO and LUMO energy levels are not significantly changed, and there is a density of states that satisfy the physisorption nature. However, HOMO and LUMO localize At the $C_{24}$ fullerene in every instance. As MER molecules have a lower HOMO level than AMP molecules—nearer to $C_{24}$ molecules—the charge transfer mechanism is considerably simpler with MER than it is with AMP. The interaction process between the complexes of the considered minimal configurations is confirmed by the alternation of the density of the states of the complexes. According to **Figure 4.5(a),** the major contribution to the Fermi level HOMO and LUMO levels comes from $C_{24}$ fullerene, which shows that AMP is minimally hybridized with $C_{24}$ fullerene in the AMP-$C_{24}$ complex[52]. Figure 5(b) makes this clear that the ketamine molecule's density of state is close to the Fermi level from DOS and molecular orbit level, and after the interaction disappears, there is a shift of the LUMO side close to the Fermi level, which is caused by the hybridization of ketamine and $C_{24}$ fullerene. The HOMO near the Fermi level in the AMP_$C_{24}$, on the other hand, is primarily contributed by $C_{24}$ fullerene, whereas the LUMO near the Fermi level is contributed by $C_{24}$ and S-N and 6-ring benzene, which is a minimal indication of hybridization with the appearance of the shoulder in the DOS of MER_$C_{24}$ (see Figure 5(c)). In **Figure 4.6**, the localization of the LUMO electron density is shown between the nitrogen

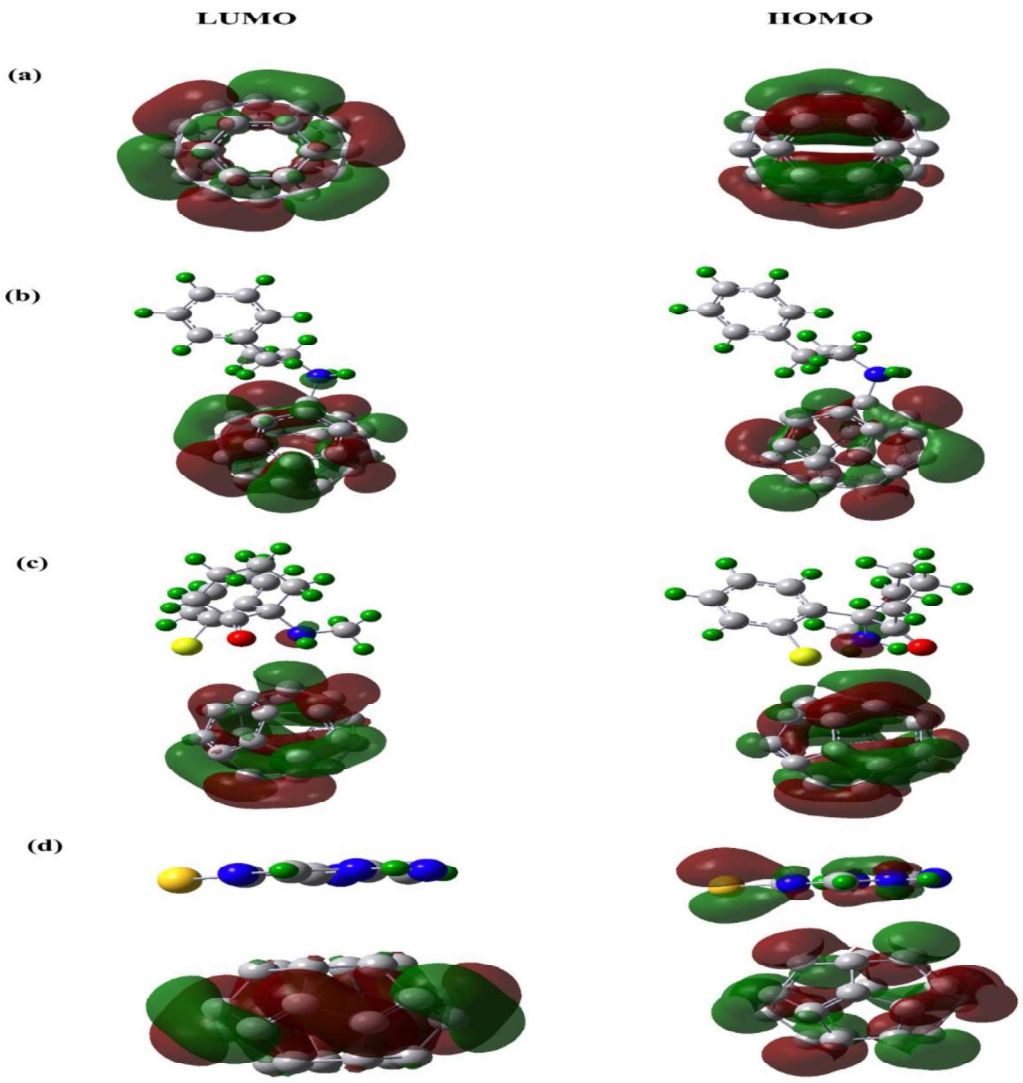


**Figure 4.6***: The electron density of the Highest Occupied Molecular Orbital (HOMO) and the Lowest Unoccupied Molecular Orbital (LUMO) for the pristine $C_{24}$ fullerene (depicted in (a)), as well as for AMP (b), KET (c), and MER (d) when adsorbed onto $C_{24}$ fullerenes, respectively.*

atom of the drug's AMP molecule and the closest carbon atom of the $C_{24}$ fullerene. This occurrence shows that AMP and $C_{24}$ fullerene interact strongly, supporting the existence of a chemical bond. HOMO and LUMO electron densities localize for the KET and MER adsorbed over $C_{24}$ fullerene, suggesting the optimal adsorption energy between them. The charge transfer process within molecules and between two interacting molecules can be understood with the help of the HOMO and LUMO orbitals. HOMO and LUMO represent the electron-donating and electron-accepting capabilities, respectively. It is clear from the $C_{24}$/AMP complexes that the Nitrogen atoms of the $NH_2$ functional group of AMP contribute to the LUMO orbital level.

While in the instance of the MER/$C_{24}$ combination, the HOMO contribution from the S atom and 6-ring benzene shows its contribution in both the HOMO and LUMO orbital levels, a similar $NH_2$ functional group does not.

### 4.3.1.5 Sensing Response

The nobleness of a chemical sensor, which related to the energy gap ($E_G$), can be pursued with great understanding using experimental sensing properties[53]. On the basis of the following equation, the $E_G$ can investigate changes in the electrical conductivity or resistivity of $C_{24}$ fullerene caused by changes in its electronic properties[54-55].

$$\sigma = AT^{3/2} \exp(-E_G/KT) \ldots\ldots\ldots\ldots\ldots\ldots (4)$$

Where A is the constant, K is the Boltzmann constant, T is the operating temperature, and σ is the electrical conductivity. Here, we calculate the sensing response using equation (4), which uses the below formula[54] to demonstrate the effectiveness of the sensing materials.

$$S = |(\sigma_1/\sigma_2)-1| = \exp(|\Delta E_G| / KT) - 1 \ldots\ldots\ldots\ldots\ldots (5)$$

Where $\Delta E_G = E^{G2} - E^{G1}$, $E^{G2}$ and $E^{G1}$ defines the energy gaps of the $C_{24}$ nanocage and the complex, respectively.

**Table 4.3:** *Computed variations in $E_G$ ($\Delta E_G$), recovery time (τ), and sensing response (S) for Adenine, Cytosine, Guanine, Thymine, and Uracil when they are adsorbed onto $C_{24}$ fullerene, respectively.*

| System | $\Delta E_G$ (eV) | τ (sec) | S |
|---|---|---|---|
| **AMP/$C_{24}$** | -0.08 | 38.29 | 18.98 |
| **KET/$C_{24}$** | 0.03 | $7.54 \times 10^{-9}$ | 2.07 |
| **MER/$C_{24}$** | 0.05 | $8.59 \times 10^{-10}$ | 5.49 |

AMP considerably changed the HOMO-LUMO band gap of the $C_{24}$ fullerene (Table 4). This causes the $E_G$ of the fullerene to alter significantly as a result of the drug AMP adsorption, revealing that the $C_{24}$ has considerable sensitivity to the drug AMP. $C_{24}$ fullerene is found to have the best sensing response to AMP based on Eq (5) at 310 K, among all the considered

drugs (**Table 4.3**). As a result of not a significant change in $E_G$ after KET and MER adsorb over $C_{24}$, the sensing performance of those molecules is poor.

#### 4.3.1.6 Recovery Time

Experimentally, recovery time is an essential characteristic for a chemical sensor that reflects the desorption process by heating the adsorbent to a higher temperature or by exposing it to UV radiation and is strongly related to interaction intensity. Higher interaction energies between molecules and adsorbent reduce the recovery time and decrease their own interactions, which makes them less ideal for use in sensing applications. As a result, a good sensor should have a suitable optimal interaction energy and interaction distance[48].

The following equation[56] yields the Recovery time (τ).

$$\tau = \upsilon_0^{-1} \exp(-E_{ad}/KT) \ldots\ldots\ldots\ldots\ldots\ldots (6)$$

Where T, K, and $\upsilon_0$, respectively, stand for temperature, Boltzmann's constant, and attempt frequency. Experimental evidence has shown that various photonic frequencies ($\upsilon_0$) or thermal energy have been employed to cause the desorption of drug and biomolecules[56]. By selecting a $\upsilon_0$ of $10^{15}$ $s^{-1}$ and a temperature of 300 K, we projected the recovery durations for the AMP, KET, and MER from the $C_{24}$ perimeter (See **Table 4.3**). The highest recovery time for the AMP drug molecule is 38.29 s, which is in accordance with significant chemisorption nature. Due to the longer Recovery time, it is possible to isolate the drug molecule AMP from the sequence of other drug molecules using the $C_{24}$ fullerene. Even for KET and MER, the interatomic distance from the $C_{24}$ fullerene is 2.49 Å and 2.95 Å, and the recovery times are $7.54\times 10^{-9}$ s and $8.59\times 10^{-10}$ s, respectively. This suggests that the medications KET and MER may be used for the best detection using the $C_{24}$ fullerene.

#### 4.3.1.7 Solvent effect:

The polarizable continuum model, or PCM approach, has been applied in the current investigation to assess the solvent's dominance since the drug/$C_{24}$ fullerene complexes truly exist biologically[57]. We reoptimized the three drug molecules, $C_{24}$ individually, and all the minimum configurations of AMP, KET, MER, and $C_{24}$ complexes in the water solvent using the DFT/B3LYP/6-31(d,p) with D3 version of Grimme's dispersion. The measured adsorption energies and sensor parameter values are listed in Table 4. The results demonstrate that the adsorption energies of the AMP/$C_{24}$ and KET/$C_{24}$ complexes relative

to the gaseous phase, which are 1.53 eV and 1.29 eV, respectively, drop when the overall energy values of the $C_{24}$ fullerene, AMP, and KET systems decrease. This is because the solvent has a larger electric permittivity[58]. Additionally, the solvent's impact causes the adsorption energy of MER/$C_{24}$ complexes to rise, which decreases sensing response and decreases recovery time in an aquatic environment. It is predicted that AMP/$C_{24}$ and KET/$C_{24}$ complexes will perform better in an aqueous environment, since lower interaction energies will result in stronger sensing responses and quicker recovery times (see **Table 4.4**). The following equation has been used to compute the solvation energies ($\Delta E_{sol}$) in order to predict the solubility of the drug molecules in water[59].

$$\Delta E_{sol} = E_{sol} - E_{gas} \quad \text{.....(7)}$$

$E_{sol}$ and $E_{gas}$ are the system's energy in the water solvent and gas, respectively. The measured $E_{sol}$ for the $C_{24}$ fullerene is -0.017 eV, while it is -0.16 eV and -0.24 eV for the AMP and KET, respectively. $\Delta E_{sol}$ observed for AMP/$C_{24}$ and KET/$C_{24}$ complex is -0.69 eV and -1.13 eV respectively. AMP and KET complexes with $C_{24}$ have solvation energies that are less negative than the total solvation energies of AMP, KET, and $C_{24}$ fullerene. $C_{24}$ fullerene, AMP, and KET drug molecules appear to be highly polar and solubilized in water. On the basis of the electronic structure, the $E_G$ change for $C_{24}$ fullerene by AMP, KET and MER increases in water, 0.16,0.26 and 0.03 eV respectively, when compared to gas. The $C_{24}$ fullerene is highly to solvent medium as its sensing response has increased from 18.98 and 2.07 in the gas phase to 7310.04 and 4964.69 in water respectively. Sensing response, however, decreased in the case of the MER drug (2.19), indicating that it is less interactive in solvent media. Response (S) for AMP, KET, and MER adsorbed $C_{24}$ fullerene with solvent effect, respectively.

**Table 4.4:** *Calculated value of Adsorption energy ($E_{ad}$), LUMO energy ($E_{LUMO}$), HOMO energy ($E_{HOMO}$), HOMO-LUMO gap ($E_G$), Recovery Time ($\tau$) and Sensing Response (S) for AMP, KET, and MER adsorbed $C_{24}$ fullerene with solvent effect, respectively.*

| System | $E_{ad}$ (eV) | $E_{LUMO}$ (eV) | $E_{HOMO}$ (eV) | $E_G$ (eV) | $\tau$ (sec) | S |
|---|---|---|---|---|---|---|
| $C_{24}$ | … | -3.76 | -5.59 | 1.83 | …. | ….. |
| AMP/$C_{24}$ | -1.53 | -2.63 | -4.69 | 2.06 | $7.49\times 10^{9}$ | 7310.04 |
| KET/$C_{24}$ | -1.29 | -2.56 | -4.61 | 2.05 | $9.39\times 10^{5}$ | 4964.69 |
| MER/$C_{24}$ | -0.325 | -3.74 | -5.54 | 1.80 | $1.92\times 10^{-10}$ | 2.19 |

**Table 4.5:** *Comparison of the sensing property of $C_{24}$ fullerene with other pristine nano-materials.*

| AMP | | | |
|---|---|---|---|
| **System** | **$E_{ad}$ (eV)** | **d (ang)** | **Ref.** |
| **$C_{24}$ fullerene** | -1.02 | 1.55 | Our work |
| **$BC_3$ nano-sheet** | -0.46 | 1.70 | [27] |
| **$BC_3$ nano-tube** | -0.68 | 1.66 | |
| **$Al_{24}N_{24}$ nanocluster** | -1.53 | … | [26] |
| **$Al_{12}N_{12}$ nano-cage** | -1.01 | 2.38 | [22] |
| **$Al_{12}P_{12}$ nano-cage** | -1.26 | 3.07 | |
| **Silicon carbide nanotube (SiCNT)** | -0.37 | 2.57 | [54] |
| **$C_{60}$ Fullerene** | -0.05 | 3.21 | [23] |
| **MER** | | | |
| **System** | **$E_{ad}$ (eV)** | **d (ang)** | **Ref.** |
| **$C_{24}$ fullerene** | -0.365 | 2.95 | Our Work |
| **$B_{12}N_{12}$ nanoclusters** | -0.62 | 2.36 | [31] |
| **BN nanosheet** | -0.13 | 3.87 | [30] |
| **BN nanotube** | -0.81 | 1.64 | |
| **BN nanocluster** | -1.92 | 1.60 | |
| **$B_{24}N_{24}$ nanocage** | -0.67 | 1.65 | [29] |
| **$C_{70}$ fullerene** | -0.26 | 3.1 | [28] |
| **KET** | | | |
| **System** | **$E_{ad}$ (eV)** | **d (ang)** | **Ref.** |
| **$C_{24}$ fullerene** | -0.423 | 2.49 | Our Work |
| **Functionalized single-walled carbon nanotube-R1** | -4.16 | ….. | [32] |
| **Functionalized single-walled carbon nanotube-R2** | -4.64 | ….. | |

### 4.3.1.8 Comparison of sensing property of $C_{24}$ fullerene with other pristine nano-material

We compared the adsorption energies ($E_{ad}$) and interatomic distances (d) of illegal drug molecules AMP, KET, and MER over $C_{24}$ fullerene with previously reported studies [22-32][54]to assess the versatility of pristine $C_{24}$ fullerene in terms of its sensing mechanism

toward the drug molecules. **Table 4.5** makes it evident that the drug AMP has a relatively poor adsorption energy toward the pristine $C_{60}$ fullerene with the wide interatomic distances, making it unsuitable for drug detection. A chemosorption with a significant interatomic distance is seen for the pristine $Al_{12}N_{12}$ and $Al_{12}P_{12}$ nano-cages, which restricts their utility for AMP drug detection. However, in contrast, our findings show that the $C_{24}$ fullerene has a higher adsorption energy at the right interatomic lengths. Additionally, compared to functionalized single-walled carbon nanotube[32] and $C_{70}$ fullerene,[28] KET and MER drug molecules had shorter interatomic distances and the best adsorption energy, suggesting that they are not suitable for drug detection purposes. Due to its physisorption towards these molecules and short recovery time, $C_{24}$ fullerene may be a good candidate for sensing applications for KET and MER drug molecules, while AMP drug molecules may be removed.

### 4.3.2 Molecular Dynamics Simulation

The equilibrium and stability of drug molecules and $C_{24}$ fullerene complexes in the aqueous environment explicitly at room temperature (310K) are assured using molecular dynamics modeling, which is a very helpful tool. We noted from the DFT-PCM study previously described that the drug molecules' sensitivity to $C_{24}$ fullerene increases in the aqueous environment, which also improves $C_{24}$ fullerene's sensing response in comparison to the gaseous phase. Investigating such complexes' dynamical stability in a water environment is therefore required. Here, we have estimated the temperature, total energy, and root mean square deviation (RMSD) of the complexes up to 50 ns. **Figure 4.7** shows the

**Table 4.6:** *Detail of the simulation boxes which used in this work*

| System | No. of Drug Molecules | No. of $C_{24}$ fullerene | No. of water molecule | Dimension of the cubic box(nm) |
|---|---|---|---|---|
| **AMP/$C_{24}$** | 4 | 2 | 4998 | 6.00 × 6.00 ×6.00 |
| **KET/$C_{24}$** | 4 | 2 | 5677 | 6.00 × 6.00 ×6.00 |
| **MER/$C_{24}$** | 4 | 2 | 4065 | 6.00 × 6.00 ×6.00 |

snapshots from the MD simulation of AMP, KET, and MER drug molecules with $C_{24}$ fullerene. The RMSD curves for the entire system against time are shown in **Figure 4.8(a)** in order to

determine the systems' initial equilibrium state. RMSD curves are shown for the three chosen systems AMP/$C_{24}$, KET/$C_{24}$, and MER/$C_{24}$. A close examination of the RMSD curves indicates

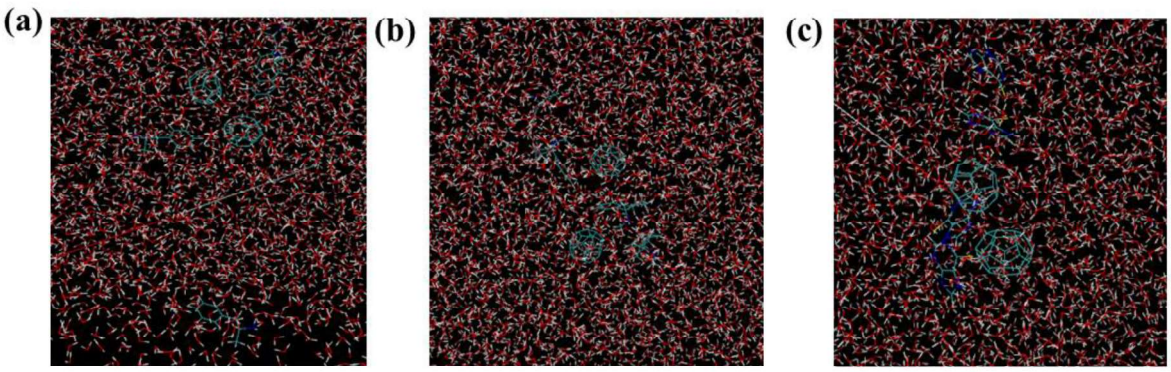


**Figure 4.7:** *Captured moments in time for the simulation systems of (a) $C_{24}$/AMP, (b) $C_{24}$/KET, and (c) $C_{24}$/MER..*

that the all-equilibrated system saw very little variation throughout the 50 ns trajectory, which was about 4 nm. Comparing the AMP/$C_{24}$ system to KET/$C_{24}$ and MER/$C_{24}$ during the simulation, RMSD fluctuation for all three systems was kept to a minimum. To comprehend how drug molecules are distributed around $C_{24}$ fullerene surfaces in water solvent for three systems, the radial distribution (RDF), or g(r), between drug molecules and $C_{24}$ fullerenes has

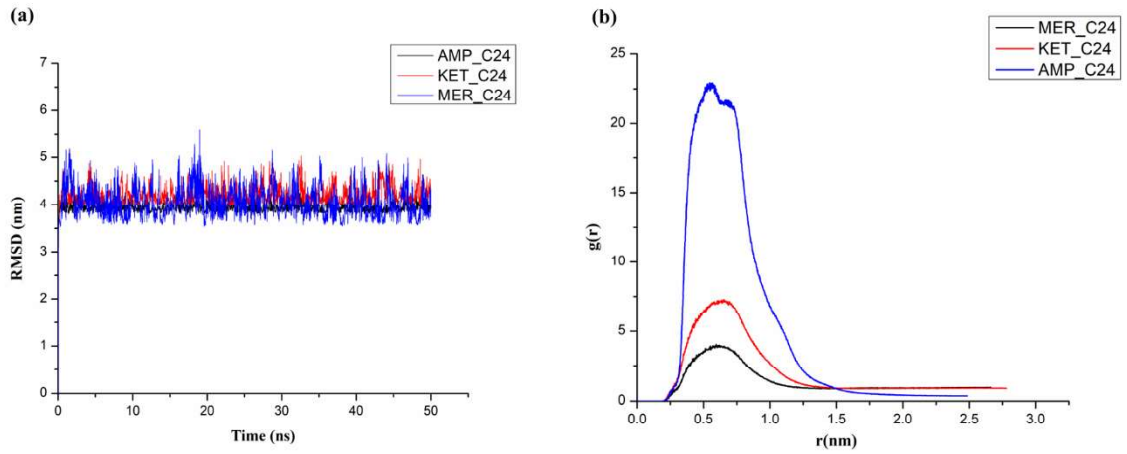


**Figure 4.8:** *(a) Plots depicting the Root Mean Square Deviation (RMSD) over time for the drug molecules in interaction with $C_{24}$ fullerene, and (b) a comparative analysis of the radial distribution (g(r)) of drug molecules in proximity to the surfaces of $C_{24}$ fullerene, as a function of distance.*

been determined (**Figure 4.8 (b)**). Notably, the center of gravity of drug molecules and $C_{24}$ fullerenes have been plotted using the three figures. Based on the RDF graphs, we can infer that g(r) at short distances is zero due to the strong repulsive forces between drug molecules

and $C_{24}$ fullerenes. Remarkably, the larger size and heightened steric impact of the KET molecule resulted in the onset of nonzero values for g(r) occurring at a greater distance compared to the other two drug molecules, which also owe their delayed effect to their size and steric attributes. Due to the increased interaction energies of AMP and KET drug molecules with $C_{24}$ fullerene, which is compatible with DFT / PCM studies, the probability of finding the AMP and KET drug molecules surrounding the $C_{24}$ fullerene is higher than MER drug. The drug molecules are distributed over the surfaces of $C_{24}$ fullerenes in the range of 0.2–2.5 nm, as shown in **Figure 8(b)**. The RDF results show that the adsorbed drug molecules and $C_{24}$ fullerene interact strongly at a distance of 0.5 nm for all three systems. In **Figure 4.9(a) and (b)**, the fluctuation of total energy and temperature vs. simulation time steps of the drug/$C_{24}$ fullerene complexes has been plotted. During the simulation durations, we see that the total energies of three complexes approach the equilibrium state. The temperature variation graph shows that the simulated temperature of 310K was maintained for all complexes during the simulation. According to these results, the complexes approach equilibrium and adsorption for the drug/$C_{24}$ complexes occurs at room temperature during 50 ns. Fig.9(a) shows the maximum average total energy of the KET/$C_{24}$ and AMP/$C_{24}$ complexes -172193 and 152604 KJ/mol, respectively. Which are consistent with DFT/PCM results. In the water environment, KET/$C_{24}$ and AMP/$C_{24}$ showed greater stability.

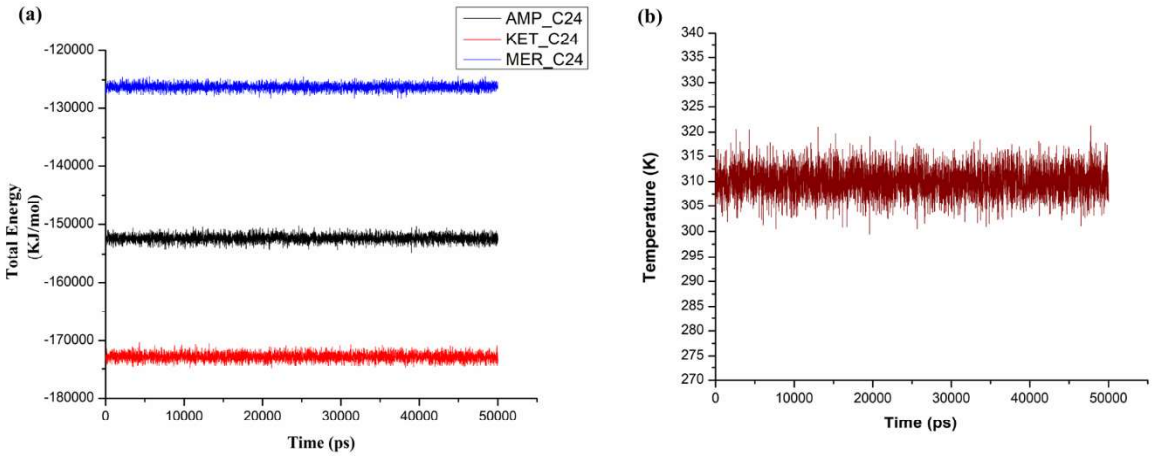


**Figure 4.9:** *MD simulation plots for the (a) Total Energy and (b) Temperature for the drug molecules/$C_{24}$ against the time simulation.*

## 4.4 Conclusions

Using the DFT-D3 method in conjunction with solvents, the present study investigated and analyzed the adsorption process of drug molecules on $C_{24}$ fullerene. According to our

findings, AMP and fullerene interact strongly in the gas phase, resulting in longer recovery times and stronger sensing responses. To put it differently, $C_{24}$ fullerene can function as a chemical sensor to isolate AMP from a blend of various pharmacological compounds. Due to the physisorption nature of the adsorption of KET and MER on $C_{24}$ fullerene, shorter recovery durations of $10^{-9}$ and $10^{-10}$ s were observed and an appreciable sensing response was observed. The interaction strengths and atomic separations between $C_{24}$ and the drugs KET and MER are highly favorable, making $C_{24}$ a suitable option for detecting these substances. Moreover, in aqueous environments, the AMP and KET complexes exhibit increased reactivity and stability, as their adsorption energy rises compared to gaseous phases, primarily attributable to the influence of the solvent. The pharmaceutical substances AMP and KET significantly accelerated the sensing response and recovery time. The removal of these medication compounds (AMP and KET) is thus possible using $C_{24}$ fullerene in the water phase. As the solvent effect reduces the interaction energy of MER drug molecules, the MER/$C_{24}$ complex becomes less reactive and has a shorter recovery time, suggesting it can be used to detect MER.

In the water environment condition at room temperature (310K), the molecular dynamics simulation indicates that the complexes are well equilibrated and quite stable. A RDF plot also indicates that the drug molecules are well distributed across the $C_{24}$ fullerene within acceptable distances, which supports the DFT results that indicate adsorption mechanisms.

As a result of the combination of DFT and MD simulation results, we concluded that $C_{24}$ fullerene would be an excellent choice for removing AMP and KET drug molecules in water environments and for detecting MER drug molecules at room temperature.

**References:**

1 J. Lenika and C. Wardak, *Procedia Eng.*, 2012, **47**, 144–147.

2 X. Li, P. Du, W. Zhang and L. Zhang, *Curr. Opin. Environ. Sci. Heal.*, 2019, **9**, 73–76.

3 F. MERZ, *United Nations Off. Drugs Crime World Drug Rep. 2017*, 2017, 85–86.

4 M. Carvalho, H. Carmo, V. M. Costa, J. P. Capela, H. Pontes, F. Remião, F. Carvalho and M. De Lourdes Bastos, *Arch. Toxicol.*, 2012, **86**, 1167–1231.

5 C. Sui, Q. Tu, N. Chen, B. Yan, Z. Lu, Z. Xu and Y. Zhang, *Spectrosc. Lett.*, 2018, **51**,

403–413.

6 R. Kohrs and M. E. Durieux, *Anesth. Analg.*, 1998, **87**, 1186–1193.

7 N. A. Anis, S. C. Berry, N. R. Burton and D. Lodge, *Br. J. Pharmacol.*, 1983, **79**, 565–575.

8 L. Wang and Z. Zhang, *Talanta*, 2008, **76**, 768–771.

9 M. Keyvanfard, V. Khosravi, H. Karimi-Maleh, K. Alizad and B. Rezaei, *J. Mol. Liq.*, 2013, **177**, 182–189.

10 Z. Chen, G. Zhang, X. Chen, J. Chen, J. Liu and H. Yuan, *Biosens. Bioelectron.*, 2013, **41**, 844–847.

11 R. Ahmadi, *Int. J. Nano Dimens.*, 2018, **9**, 325–335.

12 W. M. Mullett, *J. Biochem. Biophys. Methods*, 2007, **70**, 263–273.

13 R. D. Espy, S. F. Teunissen, N. E. Manicke, Y. Ren, Z. Ouyang, A. Van Asten and R. G. Cooks, *Anal. Chem.*, 2014, **86**, 7712–7718.

14 T. Baciu, I. Botello, F. Borrull, M. Calull and C. Aguilar, *TrAC - Trends Anal. Chem.*, 2015, **74**, 89–108.

15 M. L. Ochoa and P. B. Harrington, *Anal. Chem.*, 2004, **76**, 985–991.

16 J. W. C. Alffenaar, E. M. Jongedijk, C. A. J. Van Winkel, M. Sariko, S. K. Heysell, S. Mpagama and D. J. Touw, *J. Antimicrob. Chemother.*, 2021, **76**, 423–429.

17 H. Dai, Y. Wang, X. Wu, L. Zhang and G. Chen, *Biosens. Bioelectron.*, 2009, **24**, 1230–1234.

18 H. H. Lin, Y. C. Li, C. H. Chang, C. Liu, A. L. Yu and C. H. Chen, *Anal. Chem.*, 2012, **84**, 113–120.

19 Y. Deng and G. Feng, *Anal. Chem.*, 2020, **92**, 14667–14675.

20 N. Ding, K. Liu, Y. Qi, C. Shang, X. Chang and Y. Fang, *Sensors Actuators, B Chem.*, 2021, **340**, 129964.

21 K. Vytřas, *J. Pharm. Biomed. Anal.*, 1989, **7**, 789–812.

22 H. R. A. El-Mageed and M. A. A. Ibrahim, *J. Mol. Liq.*, 2021, **326**, 115297.

23 S. Bashiri, E. Vessally, A. Bekhradnia, A. Hosseinian and L. Edjlali, *Vacuum*, 2017, **136**, 156–162.

24 A. Qu and Y. Lin, *Phys. Lett. Sect. A Gen. At. Solid State Phys.*, 2020, **384**, 126726.

25 Y. Yang, A. Sun and M. Eslami, *Phys. E Low-dimensional Syst. Nanostructures*, 2021, **125**, 114411.

26 M. M. R. Nayini, H. Sayadian, N. Razavipour and M. Rezazade, *Inorg. Chem. Commun.*, 2020, **121**, 108237.

27 A. R. Moosavi-zare, M. Abdolmaleki, H. Goudarziafshar and H. Soleymanabadi, *Inorg. Chem. Commun.*, 2018, **91**, 95–101.

28 Y. Yang, A. Sun and W. Gu, *Struct. Chem.*, 2021, **32**, 457–468.

29 Y. Yang and N. Ostadhosseini, *Phys. E Low-Dimensional Syst. Nanostructures*, 2021, **125**, 114337.

30 S. A. Aslanzadeh, *Mol. Phys.*, 2019, **117**, 531–538.

31 H. R. Abd El-Mageed and H. S. Abbas, *J. Biomol. Struct. Dyn.*, 2021, **0**, 1–20.

32 R. Zhiani, I. Razavipanah and S. Emrani, *Struct. Chem.*, 2018, **29**, 1807–1815.

33 R. Singh and J. W. Lillard, *Exp. Mol. Pathol.*, 2009, **86**, 215–223.

34 S. Bibi, S. Ur-Rehman, L. Khalid, I. A. Bhatti, H. N. Bhatti, J. Iqbal, F. Q. Bai and H. X. Zhang, *RSC Adv.*, 2022, **12**, 2873–2887.

35 S. K. Jana, D. Chodvadiya, N. N. Som and P. K. Jha, *Diam. Relat. Mater.*, 2022, **129**, 109305.

36 M. J. Frisch, Trucks, G.W., Schlegel, H.B., Scuseria, G.E., Robb, M.A., Cheeseman, J.R., *Gaussian 09, Revis. A.02, Gaussian, Inc.*, 2016, 1–2.

37 S. Grimme, J. Antony, S. Ehrlich and H. Krieg, *J. Chem. Phys.*, 10.1063/1.3382344.

38 H. J. C. Berendsen, D. van der Spoel and R. van Drunen, *Comput. Phys. Commun.*, 1995, **91**, 43–56.

39 A. D. Mackerell, N. Banavali and N. Foloppe, *Biopolymers*, 2001, **56**, 257–265.

40 P. Mark and L. Nilsson, *J. Phys. Chem. A*, 2001, **105**, 9954–9960.

41 G. Bussi, D. Donadio and M. Parrinello, *J. Chem. Phys.*,10.1063/1.2408420.

42 B. Hess, H. Bekker, H. J. C. Berendsen and J. G. E. M. Fraaije, *J. Comput. Chem.*, 1997, **18**, 1463–1472.

43 T. Darden, D. York and L. Pedersen, *J. Chem. Phys.*, 1993, **98**, 10089–10092.

44 K. S. William Humphrey, Andrew Dalke, *Jounal Mol. Graph.*, 1996, **14**, 33–38.

45 C. A. Celaya, L. F. Hernández-Ayala, F. Buendía Zamudio, J. A. Vargas and M. Reina, *J. Mol. Liq.*,10.1016/j.molliq.2021.115528.

46 M. Rakib Hossain, M. Mehade Hasan, S. Ud Daula Shamim, T. Ferdous, M. Abul Hossain and F. Ahmed, *Comput. Theor. Chem.*, 2021, **1197**, 113156.

47 V. Nagarajan and R. Chandiramouli, *Mol. Phys.*,10.1080/00268976.2021.1936248.

48 M. A. Hossain, M. R. Hossain, M. K. Hossain, J. I. Khandaker, F. Ahmed, T. Ferdous and M. A. Hossain, *Chem. Phys. Lett.*, 2020, **754**, 137701.

49 M. Shahabi and H. Raissi, *J. Incl. Phenom. Macrocycl. Chem.*, 2015, **84**, 99–114.

50 A. Hosseinian, E. Vessally, S. Yahyaei, L. Edjlali and A. Bekhradnia, *J. Clust. Sci.*, 2017, **28**, 2681–2692.

51 R. Chandiramouli, A. Srivastava and V. Nagarajan, *Appl. Surf. Sci.*, 2015, **351**, 662–672.

52 V. Nagarajan, R. Bhuvaneswari and R. Chandiramouli, *J. Mol. Graph. Model.*, 2023, **119**, 108395.

53 A. Ahmadi Peyghan, N. L. Hadipour and Z. Bagheri, *J. Phys. Chem. C*, 2013, **117**, 2427–2432.

54 Y. Yang, A. Sun and M. Eslami, *Phys. E Low-Dimensional Syst. Nanostructures*, 2021, **125**, 114411.

55 P. Dipak, D. C. Tiwari, A. Samadhiya, N. Kumar, T. Biswajit, P. A. Singh and R. K. Tiwari, *J. Mater. Sci. Mater. Electron.*, 2020, **31**, 22512–22521.

56 H. Rahman, M. R. Hossain and T. Ferdous, *J. Mol. Liq.*, 2020, **320**, 114427.

57 M. Cossi, V. Barone, R. Cammi and J. Tomasi, *Chem. Phys. Lett.*, 1996, **255**, 327–335.

58 M. Shahabi and H. Raissi, *J. Incl. Phenom. Macrocycl. Chem.*, 2016, **86**, 305–322.

59 J. Jiang, T. Yan, D. Cui, J. Wang, J. Shen, F. Guo and Y. Lin, *J. Mol. Liq.*, 2020, **315**, 113741.